1-7-2018

Numerical Algorithm for Wing-Structure Design

Jeffrey D. Taylor
Utah State University, jeffdtaylor3891@gmail.com

Douglas F. Hunsaker
Utah State University, doug.hunsaker@usu.edu

James J. Joo
U.S. Air Force Research Laboratory

Recommended Citation

Taylor, J. D., and Hunsaker, D. F., and Joo, J. J., "Numerical Algorithm for Wing-Structure Design," AIAA 2018-1050, 2018 AIAA Aerospace Sciences Meeting, Kissimmee, Florida, 8-10 January, 2018.

Numerical Algorithm for Wing-Structure Design

J. D. Taylor,* D. F. Hunsaker,†
Utah State University, Logan, Utah, 84322-4130

and

J. J. Joo‡
U.S. Air Force Research Laboratory, Wright-Patterson Air Force Base, OH, 45433-7402

Low-fidelity aerostructural optimization routines have often focused on determining the optimal spanloads for a given wing configuration. Several analytical approaches have been developed that can predict optimal lift distributions on rectangular wings with a specific payload distribution. However, when applied to wings of arbitrary geometry and payload distribution, these approaches fail. Increasing the utility and accuracy of these analytical methods can result in important benefits during later design phases. In this paper, an iterative algorithm is developed that uses numerical integration to predict the distribution of structural weight required to support the bending moments on a wing with arbitrary geometry and payload distribution. It is shown that the algorithm's predictions for the structural weight of a rectangular test wing match those found using an analytical approach. The structural weight distribution for a spanwise-constant non-structural weight distribution is also found. Coupling the algorithm with an optimization routine, the optimal lift distributions for the rectangular test wing are found and are shown to match analytical results. Finally, the optimal lift distributions for a test wing configuration with a spanwise-constant non-structural weight distribution are found using the algorithm.

Nomenclature

A = beam cross-sectional area
A_n = Fourier coefficients in the lifting-line solution for the section-lift distribution, Eq. (1)
B_n = Fourier coefficients in the lifting-line solution for the dimensionless section-lift distribution, Eq. (3)
b = wingspan
C_σ = shape coefficient for stress-limited design, Eq. (25)
c = local wing section chord length
D_i = wing induced drag
f_{n_m} = maneuvering-flight bending moment function for Runge-Kutta integration, Eq. (43)
f_{n_g} = hard-landing bending moment function for Runge-Kutta integration, Eq. (44)
h = height of the beam cross-section
h_f = flange height (i.e., vertical thickness) of the I-beam cross-section
h_i = inside height of the box beam cross-section
I = beam section moment of inertia
L = total wing lift
$\widetilde{L}$ = local wing section lift
m = number of nodes for discretized wing
$\widetilde{M_b}$ = local wing section bending moment

*Graduate Student, Mechanical and Aerospace Engineering, 4130 Old Main Hill, AIAA Student Member.
†Assistant Professor, Mechanical and Aerospace Engineering, 4130 Old Main Hill, AIAA Senior Member.
‡Senior Research Mechanical Engineer, AFRL/RQVS, 2790 D St., AIAA Senior Member.

n_a = load factor in g's
n_g = limiting load factor at the hard-landing design limit
n_m = limiting load factor at the maneuvering-flight design limit
S = wing planform area
S_b = proportionality coefficient between the weight of the wing structure per unit span and the wing section bending moment, Eq. (24)
$t_{\max}$ = maximum airfoil section thickness
V_∞ = freestream airspeed
W = gross weight
W_n = total weight of the non-structural components
W_r = weight of the non-structural components carried at the wing root
W_s = total weight of the wing structure
$\widetilde{W}_n$ = weight of non-structural components per unit span carried within the wing
$\widetilde{W}_s$ = weight of the wing structure per unit span
w = width of the beam cross-section
w_i = inside width of the box beam cross-section
w_w = web width (i.e., horizontal thickness) of the I-beam cross-section
z = spanwise coordinate relative to the midspan
γ = specific weight of the beam material
θ = change of variables for the spanwise coordinate, Eq. (1)
κ_W = weight distribution coefficient, Eq. (30)
ρ = air density
$\sigma_{\max}$ = maximum longitudinal stress

Subscripts

j = value at section j
k = value at section k
0 = value at section 0
m = value at section m

I. Introduction

Aircraft design requires a multidisciplinary approach that encompasses several aerospace disciplines, including aerodynamics, structures, propulsion systems, and controls. The successful integration of these disciplines has been a topic of interest in recent years, leading to the growth of the field of multidisciplinary design optimization (MDO).[1] Because of its highly-coupled nature, particular emphasis has been placed on the integration of aerodynamics and structures to produce optimal wing designs. This process has been termed aerostructural optimization.

Aerostructural optimization can be thought of in three levels of fidelity: conceptual design, preliminary design, and detail design. Recent years have seen an increased interest in optimization at the detail design level. At this level, high-fidelity CFD and FEA tools are often used to model the aerodynamics and the wing structure to capture the effects of subtle variations in complex geometries and configurations. Because of the high computational costs of CFD and FEA, significant effort has been made to develop methods that decrease computation time without sacrificing fidelity.[2-5] High-fidelity methods are generally used for detail-level design of all aircraft,[6] but are sometimes used at the conceptual and preliminary design levels for unconventional geometries and structures, such as morphing trailing edge wings[7,8] and tow-steered wings.[9,10]

Although high-fidelity methods have seen significant reductions in computational time, they still carry heavy computational requirements. In the preliminary design phase, the high levels of fidelity required for detail-level design are not always necessary, and reasonable accuracy can often be attained by less complex models. In order to reduce computational requirements, a high fidelity aerodynamic or structural model may be replaced by a simpler numerical or analytical model in an aerostructural optimization routine, resulting in a multi-fidelity model.

Haftka[11] was one of the first to explore multi-fidelity aerostructural optimization. Using FEA for his structural analysis, he evaluated the aerodynamics using a Fourier series definition for lift and drag. James[12] and Jansen[13] coupled FEA with an aerodynamic panel code to optimize the Common Research Model (CRM) wing.[14] Both Dunning et al.[15,16] and Stanford et al.[17,18] also examined the CRM wing, performing wing box topology optimization under various structural and aeroelastic tailoring constraints. Using FEA for structural analysis, they favored a doublet-lattice algorithm to predict aerodynamics. Still others have used numerical lifting-line methods,[19,20] vortex-lattice methods,[21,22] and experimental data[23] to replace CFD aerodynamic solvers. In place of FEA structural models, beam models[19-22] and weight equations derived statistically,[24] using response-surface methodology,[25] or other methods[21] have been used. Multi-fidelity aerostructural optimization routines have been successfully used for a wide variety of aircraft configurations, including subsonic configurations,[15-18] supersonic transports,[26-28] and rotorcraft.[29,30]

Low-fidelity optimization routines are generally used for conceptual-level design. These routines generally involve using low-fidelity aerodynamic and structural models to determine the optimal spanwise load distribution on a wing. Prandtl[31] seems to be the first to note that the elliptic lift distribution does not necessarily minimize induced drag when structural considerations are taken into account. He found a bell-shaped lift distribution that minimized induced drag for a fixed gross weight and moment of inertia of gross weight. Several others have built upon Prandtl's work. For example, Jones[32] extended Prandtl's work to determine optimal lift distributions for a given root bending moment. Gopalarathnam and Norris[33] varied camber to find an optimal lift distribution with constraints on root bending moment. Klein and Viswanathan[34,35] found the optimal lift distribution at a given lift coefficient with constraints on both root and integrated bending moment. McGeer[36] considered aeroelastic effects. Hunsaker et al.[37] took into account total aircraft weight, including a distribution of non-structural weight in the wing to find optimal lift distributions for stress-limited rectangular wing designs with constraints on integrated bending moment.

In determining optimal spanloads, minimum drag is generally achieved by shifting the loads inboard to alleviate the moments near the wingtips, allowing for an increase in wingspan. It is important to note, however, that drag reductions are generally only achieved by a non-elliptic lift distribution if wingspan is allowed to vary. As pointed out by Iglesias and Mason,[38] Takahashi,[39] and Pate and German,[40] the optimal spanload distributions that minimize weight or that minimize induced drag during a high-load maneuver are not necessarily optimal for cruise. If such lift distributions are utilized on a fixed-geometry wing, they will result in an overall increase in induced drag over a typical flight profile.

Although low-fidelity methods are generally only used in the conceptual design phase, they are instrumental in increasing fundamental understanding of the coupling between aerodynamics and wing structure. In addition, a good first-cut design can save significant time and cost at later design phases. For these reasons, it is advantageous to increase the accuracy and applicability of low-fidelity aerodynamic optimization routines and extend their utility to later design phases. This paper extends the utility of the analytical approach taken by Hunsaker et al.[37] to straight wings with arbitrary geometries and payload distributions by developing an iterative algorithm that uses numerical integration techniques to solve for the structural weight distribution required to support the wing bending moments. The wing-structure algorithm is coupled with an optimization algorithm to determine the lift distribution that minimizes induced drag for each configuration. Structural weight predictions and optimal lift distributions are shown for an example wing with two payload distributions.

II. Analytical Formulation

The Fourier series solution to Prandtl's lifting-line theory[41,42] can be used to describe the spanwise section-circulation distribution on a lifting surface. Using this circulation in the Kutta-Joukowski Law[43,44] gives a spanwise section-lift distribution

$$\widetilde{L}(\theta) = 2b\rho V_\infty^2 \sum_{n=1}^{\infty} A_n \sin(n\theta); \qquad \theta \equiv \cos^{-1}(-2z/b) \tag{1}$$

The total lift can be described using the definitions of wing lift, aspect ratio and the classical lifting-line solution for total lift

$$L = \tfrac{1}{2}\pi b^2 \rho V_\infty^2 A_1 \tag{2}$$

Using Eqs. (1) and (2), the spanwise-lift distribution can be expressed in dimensionless form

$$\frac{b\widetilde{L}(\theta)}{L} = \frac{4}{\pi}\left[\sin(\theta) + \sum_{n=2}^{\infty} B_n \sin(n\theta)\right]; \qquad B_n \equiv \frac{A_n}{A_1}, \qquad z \equiv \frac{-b\cos(\theta)}{2} \tag{3}$$

The induced drag corresponding to the total lift in Eq. (2) can be described using the definitions of total drag, aspect ratio, and the classical lifting-line solution for induced drag

$$D_i = \frac{2(L/b)^2}{\pi\rho V_\infty^2} \sum_{n=1}^{\infty} n\frac{A_n^2}{A_1^2} \tag{4}$$

Using the definition of B_n from Eq. (3) and considering the case of steady-level flight, the induced drag from Eq. (4) can be rewritten

$$D_i = \frac{2\,(W/b)^2}{\pi\rho V_\infty^2}\left(1 + \sum_{n=2}^{\infty} nB_n^2\right) \tag{5}$$

As seen in Eq. (5), at any given operating condition, the induced drag is a function of aircraft weight, wingspan, and the Fourier coefficients, B_n. For any fixed weight and wingspan, Eq. (5) is minimized by setting $B_n = 0$ for all $n > 1$. Using these values in Eq. (3) gives the well-known elliptic lift distribution.

$$\frac{b\widetilde{L}(\theta)}{L} = \frac{4}{\pi}\sin(\theta), \qquad z \equiv \frac{-b\cos(\theta)}{2} \tag{6}$$

For configurations with fixed total weight and wingspan, the elliptic lift distribution will always give a minimum in induced drag. However, if total weight and wingspan are allowed to vary, the elliptic lift distribution does not necessarily minimize induced drag.

From Eq. (5), we see that induced drag can be reduced by increasing wingspan and decreasing weight. Neglecting structural considerations, an elliptic lift distribution on a wing with the largest possible wingspan gives the greatest efficiency. However, the maximum wingspan is limited when structural requirements are taken into account. As wingspan increases, the wing bending moments increase, and the weight of the structure required to support the bending moments must also increase. At some critical wingspan, the additional drag induced by increasing the wing weight will exceed the the drag reductions attained by increasing wingspan. The wingspan at which these two effects balance is the wingspan that minimizes induced drag for a given lift distribution.

Lift distributions that shift the spanwise-lift distribution inboard alleviate the bending moments near the wingtips. This allows for a larger optimal wingspan than that allowed by the elliptic lift distribution for the same gross lift and gross weight. However, such lift distributions are achieved using non-zero values of B_n. As seen in Eq. (5), any non-zero value of B_n increases induced drag. The tradeoff between the drag induced by a non-elliptic lift distribution and the reduction in induced drag achieved by a larger optimal wingspan results in some non-elliptic lift distribution and optimal wingspan that minimize induced drag for a given weight. Prandtl's work in 1933[31] exploited this tradeoff for a rectangular wing with constrained total lift and moment of inertia of total lift to find a bell-shaped lift distribution that allowed a wingspan increase of 22.5 percent and a drag decrease of 11.1 percent. Hunsaker et al.[37] found a lift distribution for the stress-limited design of a rectangular wing that allowed a wingspan increase of 4.98 percent and drag reduction of 4.25 percent. An brief overview of these analytical approaches is given in the following sections.

A. Prandtl's Formulation

Prandtl developed the analytical relations that led to his optimal lift distribution by assuming that the section bending moment on a wing is a function of only the lift distribution, as shown in Fig. 1. Using this assumption, the section bending moment can be written

$$\widetilde{M}_b(z) = \int_{z'=z}^{b/2} \widetilde{L}(z')(z'-z)dz', \quad \text{for } z \geq 0 \tag{7}$$

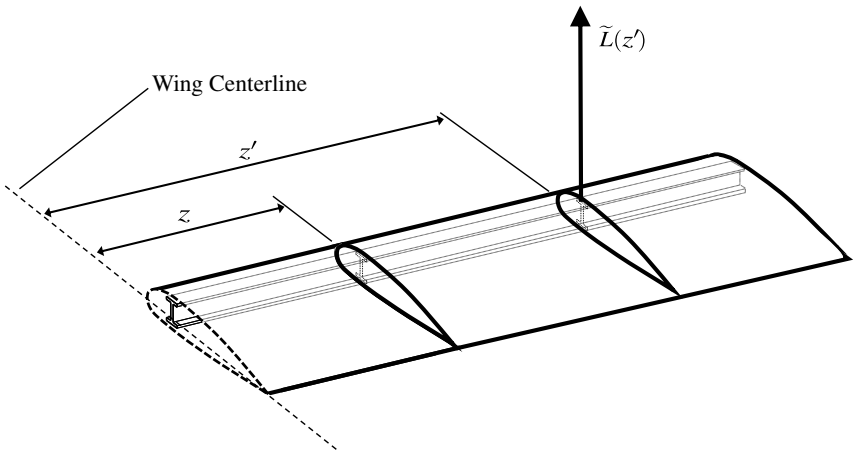

Fig. 1 Schematic of forces at spanwise location $z = z'$ contributing to the bending moment at the spanwise location z as assumed by Prandtl.[31]

In order to determine the weight of the wing structure required to support these bending moments, Prandtl[31] assumed that the section bending moments are related to the section structural weight by a spanwise-invariant proportionality constant

$$\widetilde{W}_s(z) = \frac{\widetilde{M}_b(z)}{S_b} \tag{8}$$

The total structural weight can be determined by integrating the section structural weight across the full span

$$W_s = \int_{z=-b/2}^{b/2} \widetilde{W}_s(z)dz \tag{9}$$

Using Eqs. (7) and (8) in Eq. (9) for steady level flight with any spanwise-symmetric lift distribution, and enforcing the assumption that the proportionality constant is spanwise invariant gives

$$W_s = \frac{2W}{S_b b} \int_{z=0}^{b/2} \int_{z'=z}^{b/2} \frac{b\widetilde{L}(z')}{L}(z' - z)dz'dz \tag{10}$$

When the elliptic lift distribution is used, Eq. (10) can be integrated to give the structural weight required to support the bending moments produced by the elliptic lift distribution under Prandtl's[31] assumptions

$$W_s = \frac{Wb^2}{32S_b} \tag{11}$$

Prandtl[31] minimized induced drag by using a non-elliptic lift distribution. Prandtl's lift distribution can be written in dimensionless form as

$$\frac{b\widetilde{L}(\theta)}{L} = \frac{4}{\pi}\left[\sin(\theta) - \tfrac{1}{3}\sin(3\theta)\right]; \qquad z \equiv \frac{-b\cos(\theta)}{2} \tag{12}$$

Notice that Eq. (12) is in the same form as Eq. (3) where $B_2 = 0$, $B_3 = -1/3$, and $B_n = 0$ for $n > 3$. Using Prandtl's minimum drag lift distribution in Eq. (10) and integrating gives the structural weight required to support the bending moments produced by Prandtl's lift distribution under his assumptions

$$W_s = \frac{Wb^2}{48S_b} \tag{13}$$

Equations (11) and (13) can be solved to find the wingspan for any given structural weight. Solving for wingspan shows that the wingspan allowed by Prandtl's lift distribution is 22.5 percent larger than that allowed by the elliptic lift distribution. Using the wingspan found from Eq. (11) in Eq. (5) gives the drag induced by the elliptic lift distribution with the optimal wingspan

$$D_i = \frac{W^3}{16\pi\rho V_\infty^2 S_b W_s} \tag{14}$$

The drag induced by Prandtl's lift distribution is found by using the wingspan found from Eq. (13) in Eq. (5)

$$D_i = \frac{W^3}{18\pi\rho V_\infty^2 S_b W_s} \tag{15}$$

From Eqs. (14) and (15) we see that the ratio of drag induced by Prandtl's lift distribution to the drag induced by the elliptic lift distribution is 8/9, which means that for the same gross weight, Prandtl's lift distribution induces 11.1 percent less drag than the elliptic lift distribution.

B. Hunsaker's Formulation

In his predictions for bending moment, Prandtl[31] did not take into account the effect of weight distributed across the wing. However, modern aircraft often carry some non-structural weight in addition to the weight of wing structure. The body forces produced by the weight distributed in the wing can have a large impact on the optimal lift and structural weight distribution. Hunsaker et al.[37] developed predictions for optimal structural weight and lift distribution under the assumption that the total weight of an aircraft is the sum of the weight at the wing root, W_r, the non-structural weight in the wing, W_n, and the the structural weight required to support the wing bending moments, W_s, which gives

$$W = W_r + W_n + W_s \tag{16}$$

The non-structural weight used in Eq. (16) includes the weight from all non-structural components distributed in the wing, such as fuel, nacelles, engines, or payload, as shown in Fig. 2. The total non-structural weight is found by integrating the section non-structural weight, $\widetilde{W}_n(z)$, across the span

$$W_n = \int_{z=-b/2}^{b/2} \widetilde{W}_n(z)dz \tag{17}$$

Integrating the section structural weight, $\widetilde{W}_s(z)$, across the span, the total structural weight in the wing can be written

$$W_s = \int_{z=-b/2}^{b/2} \widetilde{W}_s(z)dz \tag{18}$$

In order to find closed-form analytical solutions, Hunsaker et al.[37] limited their work to a specific non-structural weight distribution that is dependent on the total weight, weight at the wing root, and structural weight distribution

$$\widetilde{W}_n(z) = (W - W_r)\frac{\widetilde{L}(z)}{L} - \widetilde{W}_s(z) \tag{19}$$

In general, however, Eq. (19) is not a good representation of the distribution of non-structural components in a wing. In fact, a wing's non-structural weight distribution rarely follows a pattern that permits closed-form evaluation. Instead, numerical methods are required to evaluate the integrals in Eqs. (17) and (18) if an arbitrary non-structural weight distribution is considered.

Whereas Prandtl[31] assumed that the bending moments produced on a wing are a function of the lift distribution alone, Hunsaker et al.[37] also took into account the bending moments caused by the weight of the wing structure and all non-structural components. In addition, they added a provision to account for the possibility of a load factor. Figure 3 shows a schematic of the forces that contribute to the section bending moment under the assumptions made by Hunsaker et al.[37] Considering the lift distribution along with the

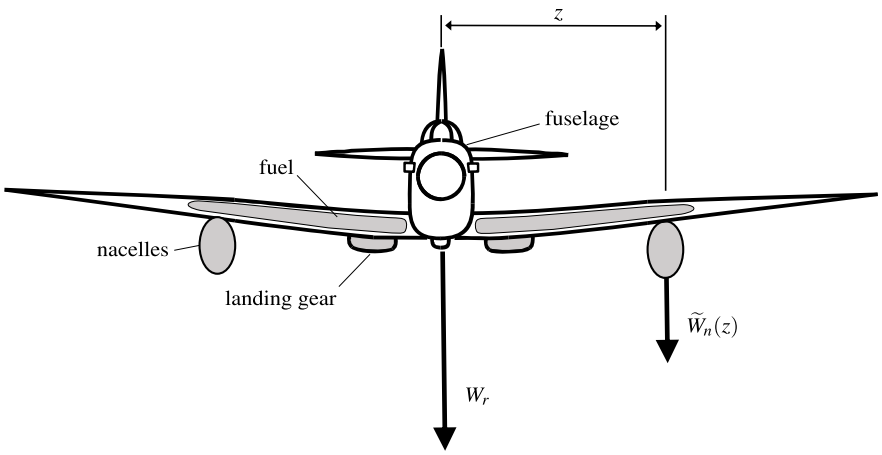

Fig. 2 Schematic of the distribution of non-structural components for an example aircraft configuration.

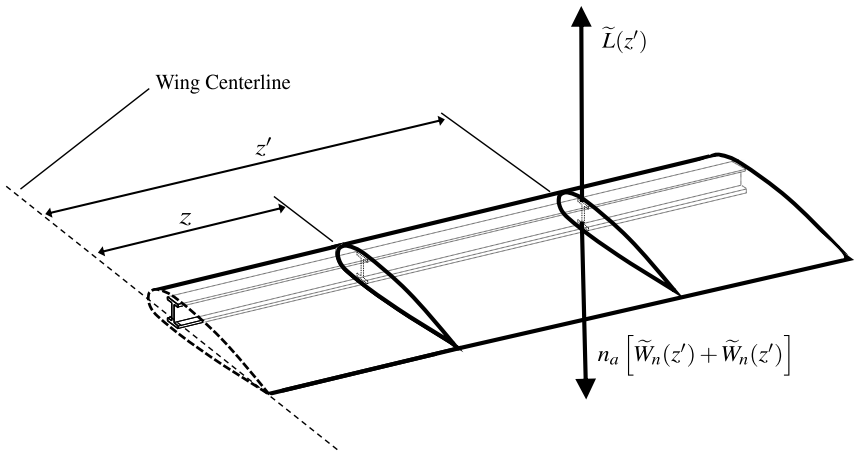

Fig. 3 Schematic of forces at spanwise location $z = z'$ contributing to the bending moment at the spanwise location z as assumed by Hunsaker et al.[37]

structural and non-structural weight distributions at some load factor, the section bending moment becomes

$$\widetilde{M}_b(z) = \int_{z'=z}^{b/2} \left[\widetilde{L}(z') - n_a\widetilde{W}_s(z') - n_a\widetilde{W}_n(z')\right](z'-z)\,dz', \quad \text{for } z > 0 \tag{20}$$

where the load factor, n_a, is measured in g's.

Equation (20) gives the general form of the section bending moment. In general, the load factor is used to account for the additional acceleration caused by a maneuver. Defining n_m as the maneuvering design limit, Eq. (20) can be rewritten

$$\widetilde{M}_b(z) = n_m \int_{z'=z}^{b/2} \left[W\frac{\widetilde{L}(z')}{L} - \widetilde{W}_n(z') - \widetilde{W}_s(z')\right](z'-z)dz', \quad \text{for } z > 0 \tag{21}$$

In addition to maneuvers, however, the load factor can be used to account for negative acceleration caused

by a hard landing or taxi bump. If n_g is taken to be the hard-landing design limit, Eq. (20) becomes

$$\widetilde{M}_b(z) = -n_g \int_{z'=z}^{b/2} \left[\widetilde{W}_n(z') + \widetilde{W}_s(z') - \frac{W}{n_g} \frac{\widetilde{L}(z')}{L} \right] (z' - z) dz', \quad \text{for } z > 0 \tag{22}$$

When determining the weight of the wing structure required to support the bending moments, both the maneuvering and hard-landing design limit must be taken into account. The limit that gives a higher magnitude bending moment at any given section is the limit that drives the structural weight required at that section.

Like Prandtl,[31] Hunsaker et al.[37] assumed that the structural weight is related to the bending moments by a proportionality constant. However, whereas Prandtl[31] assumed that the proportionality constant is invariant across the wingspan, Hunsaker et al.[37] allowed the proportionality constant to vary at each spanwise location

$$\widetilde{W}_s(z) = \frac{|\widetilde{M}_b(z)|}{S_b(z)} \tag{23}$$

Assuming that the bending moments are fully supported by a vertically symmetric beam in pure bending, Hunsaker et al.[37] related the proportionality constant to the section geometry by

$$S_b(z) = \frac{C_\sigma \left[t_{\max}(z)/c(z) \right] c(z) \sigma_{\max}}{\gamma}; \qquad C_\sigma \equiv \frac{2I \left(h/t_{\max} \right)}{Ah^2} \tag{24}$$

where $t_{\max}(z)/c(z)$ is the maximum airfoil-thickness-to-chord ratio, $c(z)$ is the chord-length distribution, $\sigma_{\max}$ is the maximum permissible stress in the beam, γ is the specific weight of the beam material, and C_σ is the beam shape factor. The shape factor for the beam cross-sections shown in Fig. 4 are given by

$$C_\sigma = \begin{cases} \dfrac{(h/t_{\max})}{6} & \text{Rectangular Beam} \\ \dfrac{\left(1 - w_i h_i^3 / w h^3\right) (h/t_{\max})}{6 \left(1 - w_i h_i / wh\right)} & \text{Box Beam} \\ \dfrac{\left[2 \left(h_f/h \right)^3 + 6 \left(h_f/h \right) \left(1 - h_f/h \right)^2 + \left(w_w/w \right) \left(1 - 2h_f/h \right)^3 \right] (h/t_{\max})}{6 \left[2h_f/h + \left(w_w/w \right) \left(1 - 2h_f/h \right) \right]} & \text{I-beam} \end{cases} \tag{25}$$

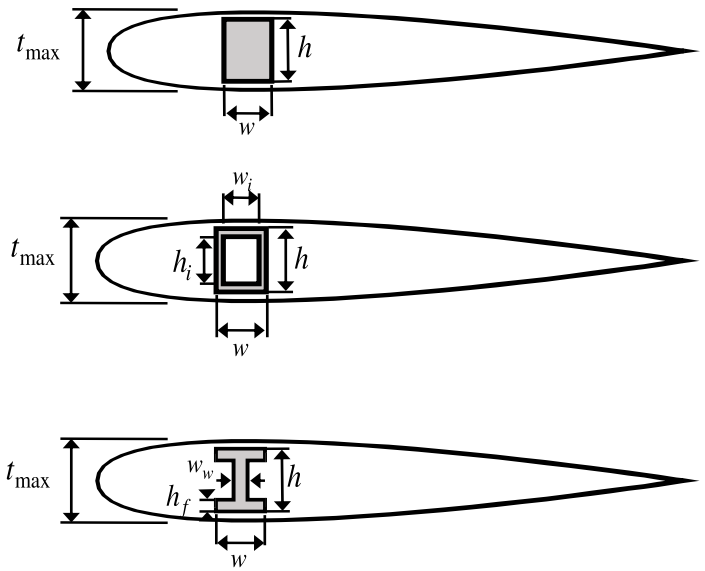

Fig. 4 Schematic of three common beam cross sections with shape factors defined in Eq. (25).

It is important to note that because the beam cross-section must fit within the airfoil thickness, the ratio $h/t_{\max}$ must be less than unity.

The total structural weight is simply the section structural weight integrated across the span. Using Eq. (23) in Eq. (18) and rewriting for a spanwise-symmetric load distribution, the total structural weight for a wing under the assumptions of Hunsaker et al.[37] is

$$W_s = 2 \int_{z=0}^{b/2} \frac{|\widetilde{M}_b(z)|}{S_b(z)} dz \tag{26}$$

where the proportionality constant, $S_b(z)$, is given by Eq. (24). In order to obtain analytical results, Hunsaker et al.[37] assumed a wing with rectangular planform shape, making the chord distribution, $c(z) = c$, and section thickness, $t_{\max}(z)/c(z) = t_{\max}/c$, constant. However, if some arbitrary non-rectangular planform is used, $c(z)$ and $t_{\max}(z)/c(z)$ are no longer spanwise invariant, and Eq. (26) must be evaluated numerically.

Using the non-structural weight distribution given by Eq. (19) in Eq. (21), Hunsaker et al.[37] were able to find analytical results for the structural weight and the optimal lift distribution. When Eq. (19) is used in Eq. (21), the maneuvering-flight section bending moment becomes

$$\widetilde{M}_b(z) = n_m W_r \int_{z'=z}^{b/2} \frac{\widetilde{L}(z')}{L} (z' - z)\, dz', \quad \text{for} \quad z \geq 0 \tag{27}$$

Similarly, using Eq. (19) in Eq. (22), the hard-landing section bending moment gives

$$\widetilde{M}_b(z) = -\left[(n_g - 1)\, W - n_g W_r\right] \int_{z'=z}^{b/2} \frac{\widetilde{L}(z')}{L} (z' - z)\, dz', \quad \text{for} \quad z \geq 0 \tag{28}$$

Notice that Eqs. (27) and (28) are directly proportional to the bending moments found by Prandtl in Eq. (7).

The total structural weight required to support the bending moments on a wing with the non-structural weight distribution given by Eq. (19) is found by using Eqs. (3), (27), and (28) in Eq. (26)

$$W_s = \frac{8\kappa_W W_r}{\pi b S_b} \int_{z=0}^{b/2} \int_{z'=z}^{b/2} \left\{ \sin\left[\cos^{-1}\left(-\frac{2z'}{b}\right)\right] + \sum_{n=2}^{\infty} B_n \sin\left[n \cos^{-1}\left(-\frac{2z'}{b}\right)\right] \right\} (z' - z)\, dz' dz \tag{29}$$

where

$$\kappa_W = \begin{cases} n_m, & W_r \geq \dfrac{n_g - 1}{n_m + n_g} W \\ (n_g - 1)\, \dfrac{W}{W_r} - n_g, & W_r < \dfrac{n_g - 1}{n_m + n_g} W \end{cases} \tag{30}$$

For any spanwise-symmetric lift distribution, the Fourier coefficients, B_n, are zero for all even n. Integrating Eq. (29) gives $B_n = 0$ for $n > 3$, and the total structural weight for a rectangular wing with a spanwise-symmetric lift distribution and the non-structural weight distribution given by Eq. (19) becomes

$$W_s = \frac{\kappa_W W_r b^2}{32 S_b} (1 + B_3) \tag{31}$$

Equation (31) can easily be solved to find the wingspan for a given structural weight, proportionality constant, weight at the wing root, and lift distribution defined by B_3 alone

$$b = \sqrt{\frac{32 S_b W_s}{\kappa_W W_r (1 + B_3)}} \tag{32}$$

Using Eq. (32) in Eq. (5) gives the corresponding induced drag

$$D_i = \frac{\kappa_W W_r W^2}{16\pi\rho V_\infty^2 S_b W_s} (1 + B_3) \left(1 + \sum_{n=2}^{\infty} n B_n^2\right) \tag{33}$$

It can be seen that Eq. (33) is minimized with

$$B_2 = 0; \quad B_3 = -1/3, \quad B_n = 0, \text{ for } n > 3 \tag{34}$$

These results, as well as those found by Prandtl,[31] assume that the optimal wingspan is obtained by extending wingspan while holding the chord constant. However, Hunsaker et al.[37] noted that it is often common for the wing loading, W/S, to be constrained by airspeed requirements. If wing loading is constrained, it is convenient to rewrite Eq. (31) in the form

$$W_s = \frac{\gamma(W/S)}{32C_\sigma(t_{\max}/c)\sigma_{\max}} \frac{\kappa_W W_r b^3}{W} (1 + B_3) \tag{35}$$

Solving for the wingspan in Eq. (35) gives

$$b = \sqrt[3]{\frac{32C_\sigma(t_{\max}/c)\sigma_{\max} W W_s}{(1 + B_3)\gamma(W/S)\kappa_W W_r}} \tag{36}$$

Using Eq. (36) in Eq. (5) gives the induced drag

$$D_i = \frac{2(1 + 3B_3^2)}{\pi\rho V_\infty^2} \left[\frac{(1 + B_3)\gamma(W/S)}{32C_\sigma(t_{\max}/c)\sigma_{\max}} \frac{\kappa_W W_r W^2}{W_s} \right]^{2/3} \tag{37}$$

Equation (37) is minimized with

$$B_2 = 0; \quad B_3 = -3/8 + \sqrt{9/64 - 1/12}, \quad B_n = 0, \text{ for } n > 3 \tag{38}$$

which, when used in Eq. (3), gives the minimum drag lift distribution for the stress-limited design of a rectangular wing with fixed wing loading

$$\frac{b\widetilde{L}(\theta)}{L} = \frac{4}{\pi} \left[\sin(\theta) + \left(\tfrac{3}{8} - \sqrt{\tfrac{9}{64} - \tfrac{1}{12}} \right) \sin(3\theta) \right]; \qquad z \equiv -\frac{b\cos(\theta)}{2} \tag{39}$$

Using Eq. (38) in Eqs. (35) and (37) gives a wingspan that is 4.98 percent larger than the wingspan allowed by the elliptic lift distribution and a drag reduction of 4.25 percent over the elliptic lift distribution for wings of equal weight.

Like Prandtl, Hunsaker et al.[37] limited their analysis to a rectangular wing. Furthermore, Hunsaker et al.[37] assumed the non-structural weight distribution from Eq. (19). The use of this non-structural weight distribution eliminates the circular dependence between the wing's structural weight distribution and the bending moments. A generalization of the analysis to non-rectangular wings with alternate non-structural weight distributions not only requires numerical integration, but it also requires the use of an iterative algorithm that predicts structural weight by converging the structural weight distribution and bending moment distribution on a wing with fixed geometry, lift distribution, and non-structural weight distribution. Such an algorithm is developed in the following section.

III. Numerical Algorithm

The selection of a numerical integration scheme is important when evaluating the integrals from the previous section. In general, any high-order numerical integration scheme will yield valid results, but in some cases, second order integration schemes, such as trapezoidal rule, may fail to converge on a finite, nonzero solution. In the following section, we use fourth-order Runge-Kutta to carry out the integration. For aerodynamic applications, it is common to evenly distribute nodes in θ and use cosine clustering to increase grid density near high-gradient regions, such as the wingtip. However, for simplicity, the following analysis assumes that the wing is discretized into m evenly-spaced spanwise segments in z, as shown in Fig. 5. The equations for a wing discretized with cosine clustering are given in the appendix. Note that when used to evaluate definite intervals at evenly-spaced intervals, fourth order Runge-Kutta is also known as Simpson's 1/3 rule.

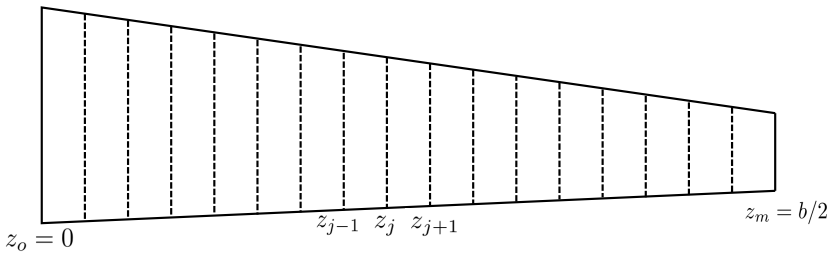

Fig. 5 Wing discretization for single semispan with even spacing in z.

If the wingspan is known and a series of Fourier coefficients, B_n, is given, Eq. (3) is fully defined. Using the nomenclature from Fig. 5, the dimensionless lift distribution given by Eq. (3) can be expressed at any section j as

$$\left(\frac{b\widetilde{L}}{L}\right)_j = \frac{4}{\pi}\left\{\sin\left[\cos^{-1}\left(-\frac{2z_j}{b}\right)\right] + \sum_{n=2}^{\infty} B_n \sin\left[n\cos^{-1}\left(-\frac{2z_j}{b}\right)\right]\right\} \tag{40}$$

Evaluation of the bending moments in Eqs. (21) and (22) requires a known dimensionless lift distribution, non-structural weight distribution, and structural weight distribution. In general, the non-structural weight distribution is known beforehand and is treated as an input to the algorithm. However, the structural weight distribution is a function of the bending moments. Therefore, some initial guess must be made for the structural weight distribution on the first algorithm iteration. For simplicity, a suitable initial guess is $\widetilde{W}_s(z) = 0$. Given a non-structural weight distribution and an initial guess for the structural weight distribution, the total non-structural weight, W_n, can be found by evaluating the integral in Eq. (17) using fourth-order Runge-Kutta

$$W_n = 2\left(z_m - z_0\right)\left[\frac{\widetilde{W}_{n_0} + 4\sum\limits_{j=1,3,5}^{m-1}\widetilde{W}_{n_j} + 2\sum\limits_{j=2,4,6}^{m-2}\widetilde{W}_{n_j} + \widetilde{W}_{n_m}}{3m}\right] \tag{41}$$

Evaluating Eq. (18) using fourth-order Runge-Kutta, the total structural weight becomes

$$W_s = 2\left(z_m - z_0\right)\left[\frac{\widetilde{W}_{s_0} + 4\sum\limits_{j=1,3,5}^{m-1}\widetilde{W}_{s_j} + 2\sum\limits_{j=2,4,6}^{m-2}\widetilde{W}_{s_j} + \widetilde{W}_{s_m}}{3m}\right] \tag{42}$$

Using Eqs. (41) and (42) in Eq. (16) gives the total aircraft weight. With the total weight known, and the non-structural and structural weight distributions defined, the maneuvering bending moment at section j can be found by using fourth-order Runge-Kutta to evaluate the integral in Eq. (21) for a given maneuvering limit, n_m

$$\widetilde{M}_{b_j} = n_m\left(z_m - z_j\right)\left[\frac{f_{n_m}(z_j) + 4\sum\limits_{k=j+1,3,5}^{m-1} f_{n_m}(z_k) + 2\sum\limits_{k=j+2,4,6}^{m-1} f_{n_m}(z_k) + f_{n_m}(z_m)}{3(m-j)}\right] \tag{43}$$

$$f_{n_m}(z_k) = \left[W\left(\frac{\widetilde{L}}{L}\right)_k - \widetilde{W}_{n_k} - \widetilde{W}_{s_k}\right]\left(z_k - z_j\right)$$

Similarly, the hard-landing bending moment at section j for a given hard-landing limit, n_g, is found from Eq. (22) by evaluating the integral using fourth-order Runge-Kutta

$$\widetilde{M}_{b_j} = -n_g \left(z_m - z_j\right) \left[\frac{f_{n_g}(z_j) + 4 \sum_{k=j+1,3,5}^{m-1} f_{n_g}(z_k) + 2 \sum_{k=j+2,4,6}^{m-1} f_{n_g}(z_k) + f_{n_g}(z_m)}{3(m-j)} \right] \tag{44}$$

$$f_{n_g}(z_k) = \left[\widetilde{W}_{n_k} + \widetilde{W}_{s_k} - \frac{W}{n_g} \left(\frac{\widetilde{L}}{L} \right)_k \right] (z_k - z_j)$$

The wing structure at section j must be built to withstand the section bending moment of greater magnitude between Eq. (43) and (44). When this bending moment is used in Eq. (23), the structural weight at section j becomes

$$\widetilde{W}_{s_j} = \frac{|\widetilde{M}_{b_j}|}{S_{b_j}} \tag{45}$$

where S_{b_j} is the proportionality constant at section j

$$S_{b_j} = \frac{C_{\sigma_j} \left(t_{\max_j}/c_j\right) c_j \sigma_{\max}}{\gamma}; \qquad C_{\sigma_j} \equiv \frac{2 I_j \left(h_j/t_{\max_j}\right)}{A_j h_j^2} \tag{46}$$

Using the new value for the structural weight calculated from Eq. (45) in Eqs. (42) and (16) gives a new guess for structural weight and total weight that can be used again in Eqs. (43) and (44). The process is repeated until the structural weight converges to some predetermined convergence criterion.

For any user-defined non-structural weight distribution and lift distribution applied to a prescribed wing geometry, the process of solving for the structural weight required to support the wing bending moments is shown in Fig. 6 and summarized as follows:

1. Use Eq. (46) with the properties of the beam to find the proportionality constant at each section.
2. Find the total non-structural weight using Eq. (41).
3. Find the total structural weight using Eq. (42). For the first iteration, assume that W_s, $\widetilde{W}_s(z) = 0$
4. Find the total weight using Eq. (16).
5. Find the moment distributions from Eqs. (43)-(44).
6. Determine which of the bending moments has the greater magnitude at each section.
7. Find the structural weight at each section by using the bending moment from step 6 in Eq. (45)
8. Repeat steps 2-7 with the new structural weight. Continue iterating until the structural weight has converged to some prescribed convergence criterion.

Using the final total weight along with the input parameters in Eq. (5), the induced drag is calculated.

This algorithm can be coupled with optimization codes to determine optimal values for a wide range of design variables under various user-defined constraints. In the following sections, we will use the algorithm described in this section to predict the structural weight and induced drag on an example wing configuration with two different non-structural weight distributions. We will also determine optimal lift distributions corresponding to each of the non-structural weight distributions.

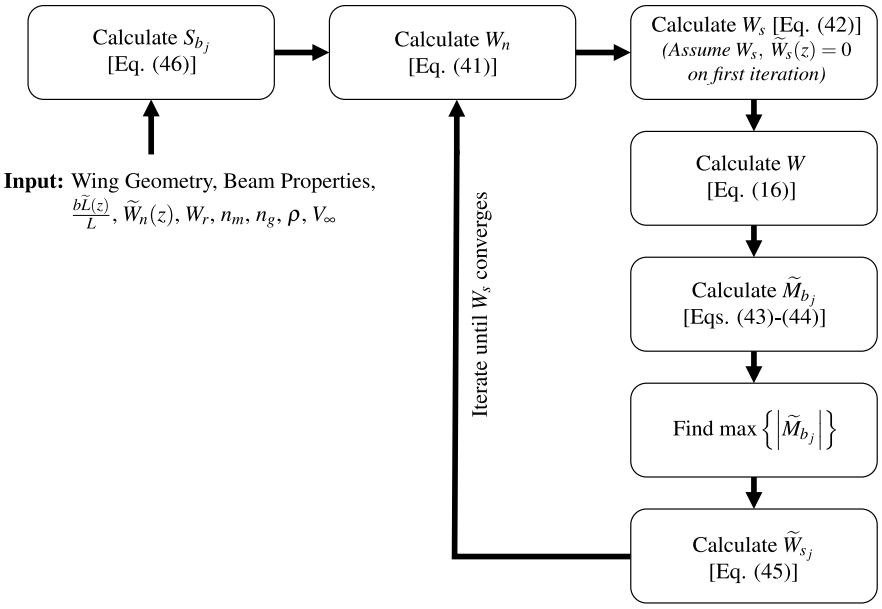

Fig. 6 Schematic of wing-structure prediction algorithm.

IV. Example Solutions

The work of Hunsaker et al.[37] provides analytical relations to predict the structural weight and optimal lift distribution for a rectangular wing with constant cross-section. These analytical relations were used to validate the results found using the wing-structure algorithm described in the previous section. The following sections compare the results for the wing-structure algorithm to the analytical relations developed by Hunsaker et al.[37] for the rectangular wing configuration defined in Table 1 with a support beam of rectangular cross-section. Note that the configuration given in Table 1 is a baseline configuration. The values shown are all held constant unless specified otherwise. We will first examine the structural weight predicted by the wing-structure algorithm using the configuration given in Table 1 and the non-structural weight distribution defined by Eq. (19) and validate them using the analytical relations developed by Hunsaker et al.[37] We will then use the algorithm to predict the structural weight for the same configuration with a spanwise-constant non-structural weight distribution.

Table 1 Properties of test wing and support beam configuration.

b [m]	c [m]	S [m^2]	$t_{\max}/c$	$\sigma_{\max}$ [Pa]	$h/t_{\max}$	γ
3.1	0.22	0.682	0.12	310×10^6	0.984	26500

W [N]	W_r [N]	n_m	n_g	ρ [kg/m^3]	V_∞ [m/s]	m
122	55	10	10	1.223	19	100

A. Hunsaker's Non-Structural Weight Distribution

The non-structural weight given by Eq. (19) was developed in order to find analytical solutions and is not intended to represent a practical non-structural weight distribution. However, in order to validate the numerical results obtained by the wing-structure algorithm, the analysis in this section uses the non-structural weight distribution given by Eq. (19) and compares the results found by the algorithm to those

found by Hunsaker et al.[37]

For this example, all of the parameters given in Table 1 are held constant. The algorithm's bending-moment predictions are found using Eqs. (43) and (44) with the fully converged structural weight distribution, non-structural weight distribution, and total weight. At each section, the wing structure must be designed to support the section moment that has greater magnitude between Eqs. (43) and (44). Figure 7 shows the distribution of structural weight predicted by the algorithm for the configuration given in Table 1 with the non-structural weight distribution specified by Eq. (19) compared to those found by Hunsaker et al.[37] using Eq. (27) or (28) in Eq. (23). Results are shown for the elliptic lift distribution from Eq. (6), Prandtl's minimum-drag lift distribution[31] from Eq. (12), and the lift distribution suggested by Hunsaker et al.[37] in Eq. (39). Notice that the structural weight distribution predicted by the algorithm agrees well with the structural weight distribution predicted by Hunsaker et al.[37] for each of the lift distributions shown.

Integrating each of the structural weight distributions shown in Fig. 7 along the span gives the total structural weight. The wing-structure algorithm calculates the drag induced by each lift distribution using Eq. (5) with the fully converged values of total weight. Table 2 compares the structural weight and induced drag calculated by the algorithm to those found by Hunsaker et al.[37]

Notice that the induced drag and total structural weight values predicted by the wing-structure algorithm match the values predicted by Hunsaker et al.[37] This suggests that the wing-structure algorithm provides a good approximation for the structural weight required to support the bending moments and the drag induced by a rectangular wing with a given all-positive spanwise-lift distribution and the non-structural weight distribution given by Eq. (19).

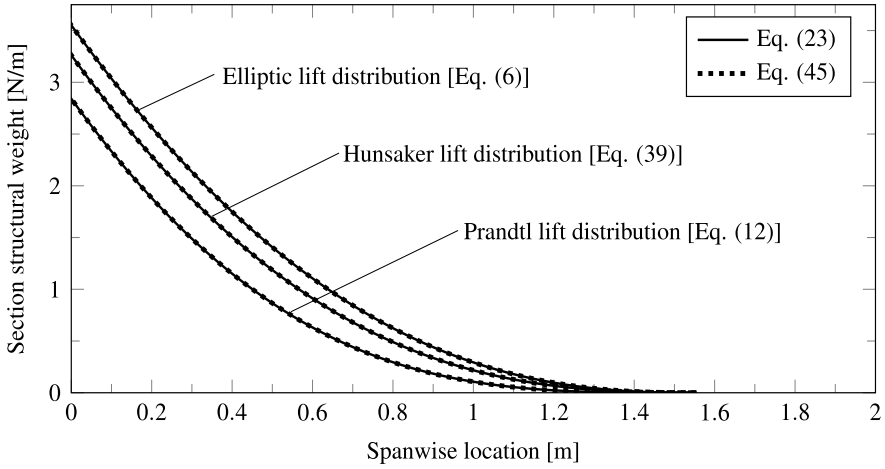

Fig. 7 Comparison of structural weight distributions predicted by the wing-structure algorithm and Hunsaker et al.[37] for the test wing defined in Table 1 with the non-structural weight distribution given by Eq. (19) and prescribed total weight.

Table 2 Comparison of structural weight and induced drag found by the wing-structure algorithm to those found by Hunsaker et al.[37] for the wing configuration given in Table 1 with the non-structural weight distribution given by Eq. (19) and prescribed total weight.

Lift Distribution	Induced Drag [N]		Structural Weight [N]	
	Algorithm	Hunsaker et al.[37]	Algorithm	Hunsaker et al.[37]
Elliptic [Eq. (6)]	2.2333	2.2333	3.2612	3.2612
Prandtl [Eq. (12)]	2.9777	2.9777	2.1741	2.1741
Hunsaker et al.[37] [Eq. (39)]	2.3565	2.3565	2.8188	2.8188

B. Even Non-Structural Weight Distribution

The non-structural weight distribution is typically driven by the non-structural components that are to be carried in a wing, and in almost all cases, will not follow Eq. (19). For a rectangular wing, an arguably more realistic alternative is to assume that the non-structural weight is distributed evenly along the wing. This section provides a more practical example than that shown in the previous section by using wing-structure algorithm to predict the structural weight for the wing configuration given in Table 1 with an even non-structural weight distribution.

Using Eq. (41), the total non-structural weight for a spanwise-constant non-structural weight distribution can be rewritten

$$W_n = 2\,(z_m - z_0)\left[\frac{\widetilde{W}_n + 4\sum\limits_{j=1,3,5}^{m-1}\widetilde{W}_n + 2\sum\limits_{j=2,4,6}^{m-2}\widetilde{W}_n + \widetilde{W}_n}{3m}\right] \tag{47}$$

where $\widetilde{W}_n$ has the same value at every section. Equation (47) can be rearranged to give

$$\widetilde{W}_n = \frac{3mW_n}{2(z_m - z_0)\,[3m-4]} \tag{48}$$

In this example, the total weight given in Table 1 is constrained. Because the total structural weight is unknown beforehand, the total non-structural weight must be allowed to vary to compensate for variations in structural weight as the algorithm converges. However, the distribution of this total weight must be defined. Because the structural weight is a function of the non-structural weight distribution, two different non-structural weight distributions will result in different values for total non-structural and structural weight.

If the gross weight and wingspan are held constant, the test configuration with an elliptic lift distribution and the spanwise-constant non-structural weight distribution given by Eq. (48) gives the same induced drag as the same configuration with the elliptic lift distribution and the non-structural weight distribution given by Eq. (19). However, using the spanwise-constant non-structural weight distribution given by Eq. (48), the wing-structure algorithm predicts a total structural weight that is 33.4 percent greater than that predicted for the non-structural weight distribution given by Eq. (19). Figure 8 shows the difference in structural weight distribution predicted by the algorithm for the wing configuration defined in Table 1 with the elliptic lift distribution and the two non-structural weight distributions given by Eqs. (19) and (48). Notice that the spanwise-constant non-structural weight distribution skews the structural weight distribution more towards the wing root than the non-structural weight distribution defined by Eq. (19). It is also interesting to note that whereas the maneuvering-flight limit constrains the structural weight if Eq. (19) is used, the

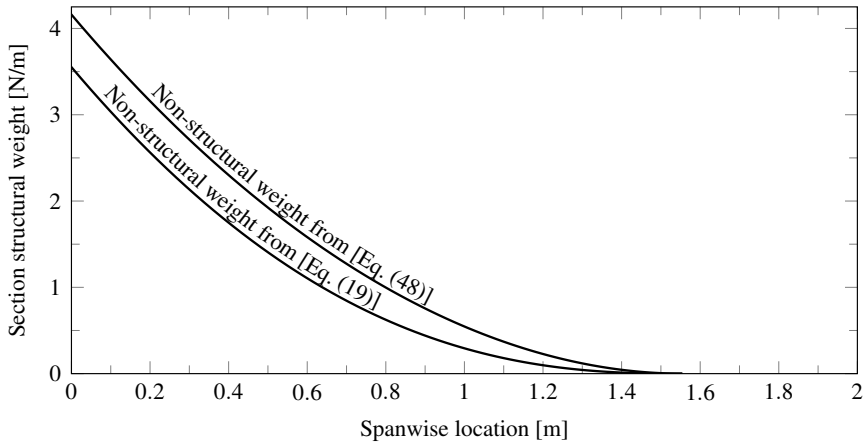

Fig. 8 Comparison of structural weight distribution predicted for the wing configuration defined in Table 1 with an elliptic lift distribution and non-structural weight distribution given by Eq. (19) vs. Eq. (48).

hard-landing limit becomes the constraining limit when Eq. (48) is used. Table 3 shows a summary of the total structural weight and induced drag obtained using the two non-structural weight distributions.

Table 3 Summary of results for induced drag and total structural weight for the wing configuration defined in Table 1 with an elliptic lift distribution and the non-structural weight distributions given by Eqs. (19) and (48).

$\widetilde{W}_n(z)$ Definition	Induced Drag [N]	Structural Weight [N]
Eq. (19)	2.2333	3.2612
Eq. (48)	2.2333	4.3348

V. Optimization

The results given in Table 2 support the assertion that the elliptic lift distribution is the optimal lift distribution for a wing with prescribed gross weight and wingspan. However, in order to find some non-elliptic optimal lift distribution for a prescribed gross weight alone, the wingspan must be allowed to vary. Optimal lift distributions for the wing configuration defined in Table 1 can be found by coupling the wing-structure algorithm with an optimization routine. Using the wing-structure algorithm as an objective function, induced drag is minimized by varying the Fourier coefficients, B_n, and wingspan, b, while holding the structural weight, W_s, constant. During a single iteration, the optimization algorithm chooses values for the wingspan and the Fourier coefficients and inputs them into the wing-structure algorithm along with the other aircraft parameters from Table 1. The wing-structure algorithm converges on the structural weight and calculates drag, which is fed back to the optimization algorithm to determine the next guesses for the wingspan and the Fourier coefficients. The process is repeated until drag is minimized. Remember that the test configuration is only used as a baseline design. If wing loading is unconstrained during optimization, the wing area will vary from the value specified in Table 1 in order to maintain constant chord length. If wing loading is constrained, the chord length and spar height will vary to maintain constant wing loading.

In this section, the wing-structure algorithm's predictions for the optimal lift distribution for a wing with the non-structural weight distribution given by Eq. (19) are validated against the analytical results found by Hunsaker et al.[37] The algorithm is then used to predict the optimal lift distributions for a wing with the spanwise-constant non-structural weight distribution. The results for the spanwise-constant non-structural weight distribution include results for both fixed total weight and fixed non-structural weight.

A. Hunsaker's Non-Structural Weight Distribution

In order to test the wing-structure algorithm's optimization results, the optimal lift distributions found using the wing-structure algorithm for the configuration given in Table 1 with the non-structural weight distribution given in Eq. (19) are compared to those found analytically by Hunsaker et al.[37] Using this non-structural weight distribution, Hunsaker et al.[37] determined that if wingspan is allowed to vary with no constraint placed on wing loading, the lift distribution that minimizes induced drag for some constant structural weight is equal to Prandtl's optimal lift distribution[31] from Eq. (12). If wing loading is constrained, however, the optimal lift distribution is given by Eq. (39).

Coupling the wing-structure algorithm with an optimization routine, the predicted optimal lift distributions for unconstrained wing loading and constrained wing loading match those found by Hunsaker et al.[37] Figure 9 shows the optimal lift distributions predicted by the algorithm with a prescribed structural weight for both the unconstrained and constrained wing loading case. Table 4 shows a comparison between the wingspan and induced drag predicted by the algorithm and those predicted by Hunsaker et al.[37]

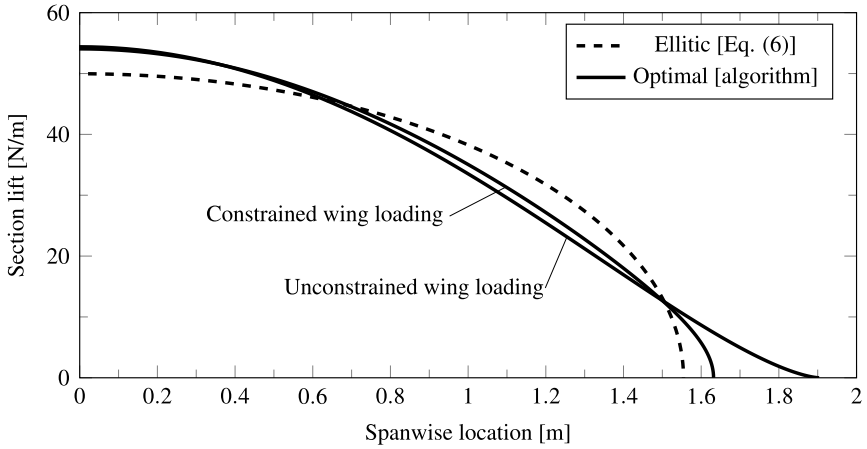

Fig. 9 Comparison between the elliptic lift distribution, Prandtl's lift distribution,[31] and the lift distribution found by Hunsaker et al.[37] on the wing defined in Table 1 with the non-structural weight distribution given in Eq. (19) and prescribed structural weight.

Table 4 Summary of results for wingspan and induced drag for the test wing given in Table 1 with the non-structural weight distribution given by Eq. (19) and prescribed structural weight.

Lift Distribution	Wingspan [m]		Induced Drag [N]	
	Algorithm	Hunsaker et al.[37]	Algorithm	Hunsaker et al.[37]
Elliptic [Eq. (6)]	3.10	3.10	2.23	2.23
Optimal [W/S unconstrained]	3.80	3.80	1.99	1.99
Optimal [W/S constrained]	3.25	3.25	2.14	2.14

B. Even Non-Structural Weight Distribution

Because the non-structural weight distribution given by Eq. (19) is not practical, the following section presents the optimization results found by the wing-structure algorithm for the configuration in Table 1 with a spanwise-constant non-structural weight distribution. When the non-structural weight distribution defined by Eq. (19) is replaced by the spanwise-constant non-structural weight distribution from Eq. (48) on the wing configuration given in Table 1, the optimization algorithm gives optimal lift distributions that vary significantly from those shown in Fig. 9. Figure 10 shows the optimal lift distributions with both constrained and unconstrained wing loading predicted by the wing-structure algorithm for the wing configuration given in Table 1 with a spanwise-constant non-structural weight distribution. The optimal lift distributions are shown plotted against the elliptic lift distribution.

It is interesting to note that whereas the optimal lift distributions for the non-structural weight distribution given in Eq. (19) are decidedly non-elliptic, the optimal lift distributions for the spanwise-constant non-structural weight distribution from Eq. (48) are both nearly elliptic. Table 5 gives a summary of the results for wingspan and induced drag. Notice that the wingspans allowed by the optimal lift distributions are nearly equal to the wingspan allowed by the elliptic lift distribution, and the induced drag for each lift distribution is within one percent of the elliptic solution. However, these results will vary depending on the value of weight carried at the wing root.

The non-zero Fourier coefficients, B_n, that define the optimal lift distributions from Fig. 10 are shown in Table 6 for $1 \leq n \leq 29$. Notice that as n increases, the magnitude of the Fourier coefficients quickly decreases. This corresponds to a decrease in each coefficient's influence on the lift distribution, structural weight, and induced drag. Figure 11 shows the change in induced drag caused by each of the Fourier coefficients from Table 6. Note that, by $n = 5$, the Fourier coefficient only influences the induced drag on the order of 10^{-5} N. These results suggest that the infinite series of Fourier coefficients that define the lift distribution could be truncated after B_3 with little loss of accuracy, and an investigation of the influence of the lift distribution

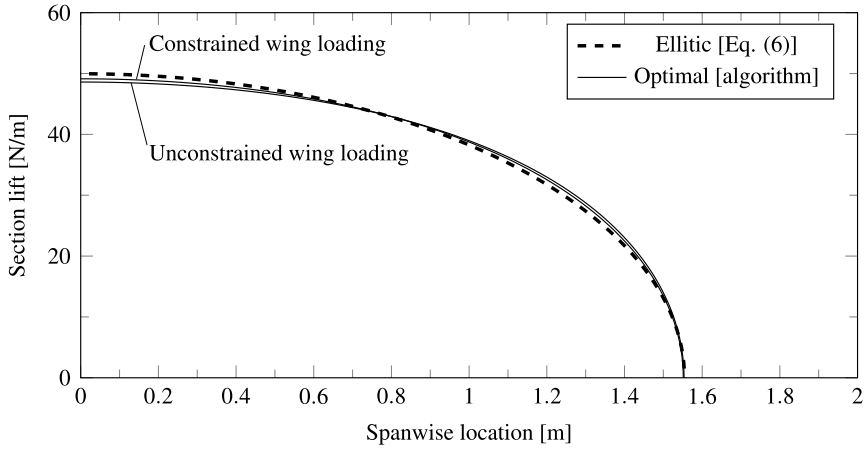

Fig. 10 Comparison between the elliptic lift distribution from Eq. (6) and the optimal lift distributions for both constrained and unconstrained wing loading predicted by the wing-structure algorithm for the wing configuration defined in Table 1 with an even non-structural weight distribution and prescribed structural weight.

Table 5 Summary of results for wingspan and induced drag for the test wing given in Table 1 with the non-structural weight distribution given by Eq. (48) and prescribed structural weight.

Lift Distribution	Wingspan [m]	Induced Drag [N]
Elliptic [Eq. (6)]	3.100	2.233
Optimal [W/S unconstrained]	3.106	2.229
Optimal [W/S constrained]	3.103	2.232

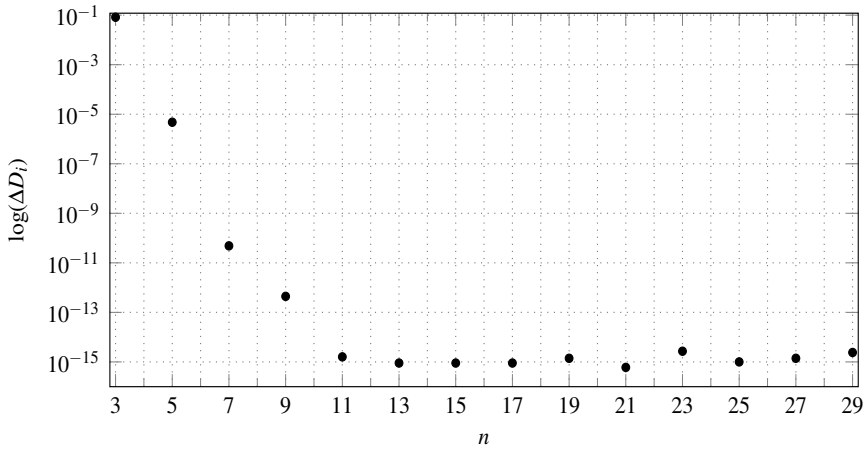

Fig. 11 The change in induced drag caused by each Fourier coefficient given in Table 6 for the case of constrained wing loading.

on induced drag can be adequately described by examining the influence of B_3 alone. Figure 12 shows the induced drag found using the maximum allowed wingspan for each lift distribution, plotted as a function of B_3, for the test configuration defined in Table 1 and an even non-structural weight distribution. As expected, the values of B_3 that minimize induced drag for the constrained and unconstrained wing-loading cases both fall very near zero.

Up to this point, our analysis has assumed that the total weight is known and that non-structural weight

Table 6 Non-zero Fourier coefficients for $1 \leq n \leq 29$ that define the optimal lift distributions for both constrained and unconstrained wing loading, as predicted by the wing-structure algorithm, for the wing configuration defined in Table 1 with an even non-structural weight distribution and prescribed structural weight.

Fourier Coefficient	Constrained Wing Loading	Unconstrained Wing Loading
B_1	1	1
B_3	1.87×10^{-2}	2.82×10^{-2}
B_5	1.10×10^{-4}	1.66×10^{-4}
B_7	2.99×10^{-7}	4.61×10^{-7}
B_9	-6.65×10^{-9}	-9.04×10^{-9}
B_{11}	-6.54×10^{-9}	-7.47×10^{-9}
B_{13}	-7.01×10^{-9}	-2.71×10^{-9}
B_{15}	-5.90×10^{-9}	-8.60×10^{-9}
B_{17}	-7.21×10^{-9}	-3.60×10^{-9}
B_{19}	-5.93×10^{-9}	-6.75×10^{-9}
B_{21}	-5.91×10^{-9}	-2.44×10^{-9}
B_{23}	-6.40×10^{-9}	-5.64×10^{-9}
B_{25}	-4.90×10^{-9}	-6.39×10^{-9}
B_{27}	-5.68×10^{-9}	-3.22×10^{-9}
B_{29}	-5.38×10^{-9}	-5.35×10^{-9}

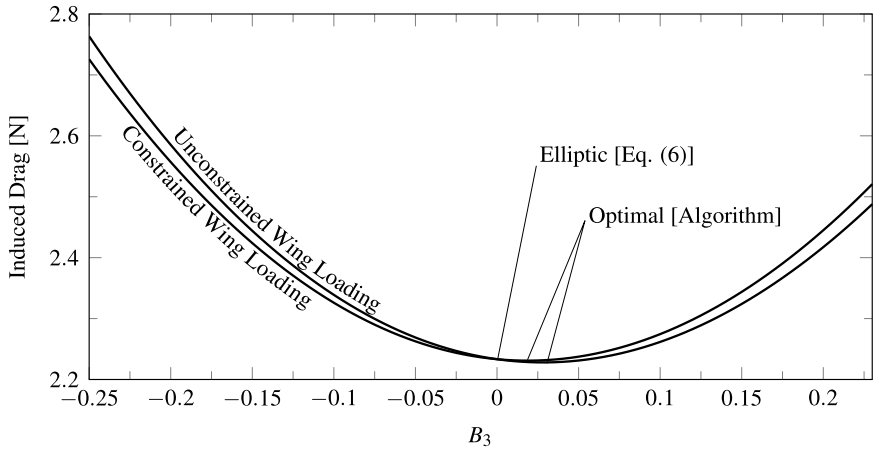

Fig. 12 The induced drag predicted for the wing defined in Table 1 with an even non-structural weight distribution and the maximum allowed wingspan for both constrained and unconstrained wing loading.

can vary to compensate for changes in structural weight. However, neglecting weight lost over time due to fuel consumption, the non-structural weight in a wing is typically constant for a given flight condition. Therefore, it is arguably more realistic to set the non-structural weight, instead of the total weight, to some fixed value. Our remaining analysis will consider the optimization of the lift distribution and wingspan for the test configuration given in Table 1 with a spanwise-constant non-structural weight distribution and fixed non-structural weight.

Relaxing the assumption that the total weight is fixed for the wing configuration given in Table 1, and distributing a prescribed total non-structural weight of $W_n = 62$ N evenly across the wing, the induced drag and structural weight predicted by the wing-structure algorithm, as a function of both wingspan and B_3,

are shown in Fig. 13. Not surprisingly, the optimization algorithm favors a very high-aspect ratio wing to minimize induced drag when carrying a fixed non-structural weight. Notice that the optimal lift distribution is obtained using a wingspan that is nearly 180 percent larger than the baseline wingspan given in Table 1.

The dashed lines in Fig. 13 represent lines of constant structural weight. In our previous analyses, the structural weight was held constant at about 4.33 N. Note that if we begin at an elliptic lift distribution ($B_3 = 0$) and the wingspan shown in Table 1, the constraint of constant structural weight requires that the optimization algorithm follow the 4.33 N structural weight contour. As expected, drag is minimized along this contour at a wingspan very near the baseline wingspan and a lift distribution with B_3 very near zero, which matches the results shown in Tables 5 and 6. However, if structural weight is allowed to vary, the optimization algorithm is no longer constrained to a single structural weight contour. Instead, minimum induced drag is achieved with a structural weight that is 38.7 percent of the total weight, and drag is reduced by about 68.5 percent over the baseline configuration from Table 1 with the elliptic lift distribution.

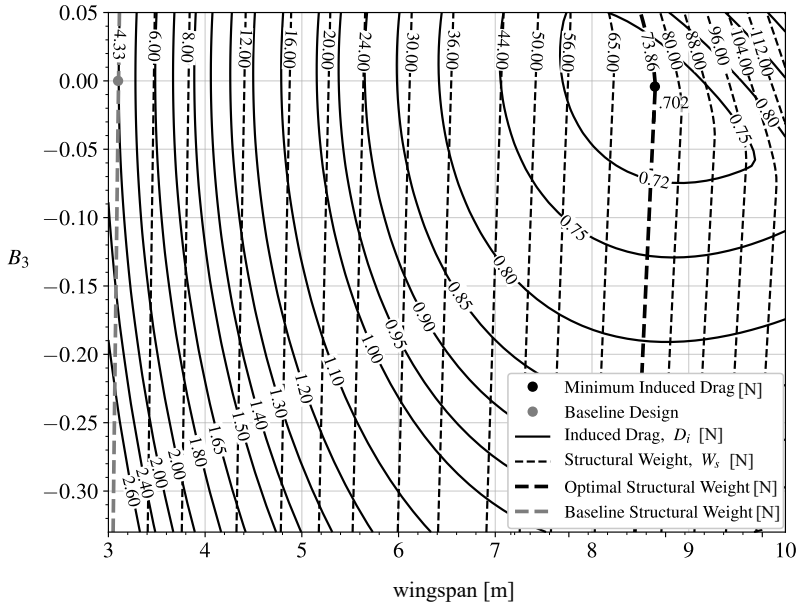

Fig. 13 Variation in induced drag and structural weight with change in wingspan and B_3 for the test configuration given in Table 1 with variable total weight and constant $W_n = 62$ N distributed evenly across the wing.

VI. Conclusions

A wide variety of low-fidelity methods have been developed to predict the optimal spanwise load distribution on an aircraft configuration. In general, these methods have shown that lift distributions that shift lift inboard alleviate moments at the wingtips, allowing a larger wingspan with no added structural weight. As seen in Eq. (5), certain lift distributions that allow larger wingspans without changing total weight may induce less drag than the elliptic lift distribution. For example, Prandtl[31] found an optimal lift distribution under the assumptions of fixed gross weight and moment of inertia of gross weight that allowed a 22.5 percent larger wingspan and produced 11.1 percent less induced drag than the elliptic lift distribution. Building on Prandtl's work, Hunsaker et al.[37] found a lift distribution under the constraints of prescribed gross weight, maximum stress, and wing loading that allowed a 4.98 percent larger wingspan and produced 4.25 percent less induced drag than the elliptic lift distribution.

The analytical approaches taken by Prandtl[31] and Hunsaker et al.[37] both assumed a straight, rectangular

wing of constant cross-section. Hunsaker et al.[37] also limited their work to the non-structural weight distribution from Eq. (19) in order to obtain analytical solutions. However, if wing geometry is allowed to vary along the span, or if some non-structural weight distribution other than that specified in Eq. (19) is used, the approaches taken by Prandtl[31] and Hunsaker et al.[37] fail to produce analytical solutions.

An algorithm that iteratively solves for the structural weight of a wing configuration with arbitrary geometry and non-structural weight distribution was developed. This algorithm makes use of a high-order numerical integration scheme to evaluate the integrals in the relations developed by Hunsaker et al.[37] It has been shown that this algorithm gives results that match those found analytically by Hunsaker et al.[37] for a rectangular wing with the non-structural weight distribution given by Eq. (19). The algorithm's predictions for structural weight and its results for optimal lift distribution with and without constraints on wing loading also match those found by Hunsaker et al.[37]

The algorithm was also used to find predictions for structural weight and the optimal lift distributions for a specific rectangular wing configuration with an even spanwise distribution of non-structural weight. For this configuration, the algorithm's results suggest that if total weight is constrained, the optimal lift distributions are nearly elliptic, and drag benefits are negligible. If the non-structural weight is constrained and total weight is allowed to vary, the optimal lift distribution is also nearly elliptic, but the optimal wingspan is nearly 180 percent larger and the induced drag is 68.5 percent less than that produced by the baseline wing configuration. It was shown that whereas the optimal lift distribution for this configuration is a function of all Fourier coefficients, the influence of each coefficient, B_n, for $n \geq 5$ on induced drag is minimal. For alternate configurations, the optimal lift distributions and drag benefits will vary from those shown in this paper.

The analysis in this paper only considered the case of a rectangular wing with two specific non-structural weight distributions. However, the methods can be applied in a similar manner to wings with arbitrary geometry and non-structural weight distribution. It is anticipated that these methods can be successfully applied to a wide variety of practical configurations in the conceptual and preliminary design stages. It is also anticipated that they will provide greater insight into the coupling of aerodynamics and wing structures.

Appendix

The numerical algorithm presented in section III of this paper assumes a wing that has been discretized with even spacing in z. However, for many clustering schemes, it is convenient to evenly space nodes in θ. Each of the equations in the development of the numerical algorithm can be rewritten in terms of θ using the change of variables from Eq. (3) and the relation

$$dz = \frac{b \sin\theta}{2} d\theta \tag{49}$$

It is also important to remember when carrying out integration that all distributions are spanwise-symmetric and that each distribution is integrated across a single semispan. This means that θ in Eq. (3) ranges between $0 < \theta < \pi/2$ with $\theta_0 = \pi/2$ and $\theta_m = 0$.

Using the change of variables from Eq. (3) and the relation given by Eq. (49), the non-dimensional lift distribution from Eq. (40) becomes

$$\left(\frac{b\widetilde{L}}{L}\right)_j = \frac{4}{\pi}\left[\sin\theta_j + \sum_{n=2}^{\infty} B_n \sin\theta_j\right] \tag{50}$$

Using the same change of variables, the total non-structural weight from Eq. (41) can be rewritten

$$W_n = -b\left(\theta_m - \theta_0\right)\left[\frac{\widetilde{W}_{n_0}\sin\theta_0 + 4\sum\limits_{j=1,3,5}^{m-1}\widetilde{W}_{n_j}\sin\theta_j + 2\sum\limits_{j=2,4,6}^{m-2}\widetilde{W}_{n_j}\sin\theta_j + \widetilde{W}_{n_m}\sin\theta_m}{3m}\right] \tag{51}$$

and the total structural weight from Eq. (42) becomes

$$W_s = -b\left(\theta_m - \theta_0\right)\left[\frac{\widetilde{W}_{s_0}\sin\theta_0 + 4\sum_{j=1,3,5}^{m-1}\widetilde{W}_{s_j}\sin\theta_j + 2\sum_{j=2,4,6}^{m-2}\widetilde{W}_{s_j}\sin\theta_j + \widetilde{W}_{s_m}\sin\theta_m}{3m}\right] \tag{52}$$

Using Eq. (49) and the change of variables from Eq. (3), the maneuvering-flight section bending moment from Eq. (43) and hard-landing section bending moment from Eq. (44) give

$$\widetilde{M}_{b_j} = \frac{n_m b}{2}\left(\theta_m - \theta_j\right)\left[\frac{f(\theta_j) + 4\sum_{k=j+1,3,5}^{m-1} f(\theta_k) + 2\sum_{k=j+2,4,6}^{m-1} f(\theta_k) + f(\theta_m)}{3(m-j)}\right] \tag{53}$$

$$f\left(\theta_k\right) = \frac{-b\sin\theta_k}{2}\left[W\left(\frac{\widetilde{L}}{L}\right)_k - \widetilde{W}_{n_k} - \widetilde{W}_{s_k}\right]\left(\cos\theta_k - \cos\theta_j\right)$$

$$\widetilde{M}_{b_j} = -\frac{n_g b}{2}\left(\theta_m - \theta_j\right)\left[\frac{g(\theta_j) + 4\sum_{k=j+1,3,5}^{m-1} g(\theta_k) + 2\sum_{k=j+2,4,6}^{m-1} g(\theta_k) + g(\theta_m)}{3(m-j)}\right] \tag{54}$$

$$g(\theta_k) = \frac{-b\sin\theta_k}{2}\left[\widetilde{W}_{n_k} + \widetilde{W}_{s_k} - \frac{W}{n_g}\left(\frac{\widetilde{L}}{L}\right)_k\right]\left(\cos\theta_k - \cos\theta_j\right)$$

The even non-structural weight distribution from Eq. (48) should also be modified for a wing with even spacing in θ. Rewriting Eq. (47) in terms of θ gives

$$W_n = -b\left(\theta_m - \theta_0\right)\widetilde{W}_n\left[\frac{\sin\theta_0 + 4\sum_{j=1,3,5}^{m-1}\sin\theta_j + 2\sum_{j=2,4,6}^{m-2}\sin\theta_j + \sin\theta_m}{3m}\right] \tag{55}$$

which can be rearranged to find the section non-structural weight for an even non-structural weight distribution in θ

$$\widetilde{W}_n = -\frac{3mW_n}{b(\theta_m - \theta_0)\left[\sin\theta_0 + 4\sum_{j=1,3,5}^{m-1}\sin\theta_j + 2\sum_{j=2,4,6}^{m-2}\sin\theta_j + \sin\theta_m\right]} \tag{56}$$

Acknowledgment

This work was partially performed during a summer faculty fellowship sponsored by the Air Force Research Laboratory. The authors wish to express their appreciation for the support of AFRL. This paper has been cleared for public release, Case Number: 88ABW-2017-5940.

References

[1]Sobieszczanski-Sobieski, J., and Haftka, R. T., "Multidisciplinary Aerospace Design Optimization: Survey of Recent Developments," *Structural Optimization*, Vol. 14, No. 1, 1997, pp. 1-23.

[2]Piperni, P., Abdo, M., Kafyeke, F. and Isikveren, A. T., "Preliminary Aerostructural Optimization of a Large Business Jet," *Journal of Aircraft*, Vol. 44, No. 5, 2007 pp. 1422-1438.

[3]Gazhlane, I., Carrier, G., Dumont, A., Marcelet, M., and Désidéri, J., "Aerostructural Optimization with the Adjoint Method," EuroGen 2011 Evolutionary and Deterministic Methods for Design, Optimization and Control, Capua, Italy, 14-16 September 2011.

[4]Kenway, G. K. W., and Martins, J. R. R. A., "Multipoint High-Fidelity Aerostructural Optimization of a Transport Aircraft Configuration," *Journal of Aircraft*, Vol. 51, No. 1, 2014, pp. 144-160.

[5]Zhang, Z. J., Khosravi, S., Zingg, D. W., "High-Fidelity Aerostructural Optimization with Integrated Geometry Parameterization and Mesh Movement," AIAA 2015-1132, 56th AIAA/ASCE/AHS/ASC Structures, Structural Dynamics, and Materials Conference, Kissimmee, Florida, 5-9 January 2015.

[6]Martins, J. R. R. A., Alonso, J. J., and Reuther, J. J., "High-Fidelity Aerostructural Design Optimization of a Supersonic Business Jet," *Journal of Aircraft* Vol. 41, No. 3, 2004, pp. 523-530.

[7]Burdette, D. A., Kenway, G. K. W., Lyu, Z., and Martins, J. R. R. A., "Aerostructural Design Optimization of an Adaptive Morphing Trailing Edge Wing," AIAA 2015-1129, 56th AIAA/ASCE/AHS/ASC Structures, Structural Dynamics, and Materials conference, AIAA SciTech Forum, Kissimmee, Florida, 5-9 January 2015.

[8]Burdette, D. A., Kenway, G. K. W., and Martins, J. R. R. A., "Aerostructural Design Optimization of a Continuous Morphing Trailing Edge Aircraft for Improved Mission Performance," AIAA 2016-3209, 17th AIAA/ISSMO Multidisciplinary Analysis and Optimization Conference, AIAA Aviation Forum, Washington, D.C., 13-17 June 2016.

[9]Brooks, T. R., Martins, J. R. R. A., and Kennedy, G. J., "High-Fidelity Aerostructural Optimization of a High Aspect Ratio Tow-steered Composite Wing," AIAA 2016-1179, 57th AIAA/ASCE/AHS/ASC Structures, Structural Dynamics, and Materials Conference, San Diego, California, 4-8 January 2016.

[10]Brooks, T. R., Martins, J. R. R. A., and Kennedy, G. J., "High-Fidelity Multipoint Aerostructural Optimization of a High Aspect Ratio Tow-steered Composite Wing," AIAA 2017-1350, 58th AIAA/ASCE/AHS/ASC Structures, Structural Dynamics, and Materials Conference, Grapevine, Texas, 9-13 January 2017.

[11]Haftka, R. T., "Optimization of Flexible Wing Structures Subject to Strength and Induced Drag Constraints, *AIAA Journal*, Vol. 14, No. 8, 1977, pp. 11061977.

[12]Janes, K. A., Kennedy, G. J., and Martins, J. R. R. A., "Concurrent Aerostructural Topology Optimization of a Wing Box," *Computers and Structures*, Vol. 134, No. 1, 2014, pp. 1-17.

[13]Jansen, P. W., Perez, R. E., and Martins, J. R. R. A., "Aerostructural Optimization of Nonplanar Lifting Surfaces," *Journal of Aircraft* Vol. 47, No. 5, 2010, pp. 1490-1503.

[14]Vassberg, J., DeHaan, M., Rivers, S., and Wahls, R., Development of a Common Research Model for Applied CFD Validation Studies, AIAA 2008-6919, 26th AIAA Applied Aerodynamics Conference, Honolulu, Hawaii, 18-21 August 2008.

[15]Dunning, P. D., Stanford, B. K., and Kim, H. A., "Aerostructural Level Set Topology Optimization for a Common Research Model Wing," AIAA 2014-0634, 10th AIAA Multidisciplinary Design Optimization Conference, National Harbor, Maryland, 13-17 January 2014.

[16]Dunning, P. D., Stanford, B. K., and Kim, H. A., "Level-Set Topology Optimization with Aeroelastic Constraints," AIAA 2015-1128, 56th AIAA/ASCE/AHS/ASC Structures, Structural Dynamics, and Materials Conference, Kissimmee, Florida, 5-9 January 2015.

[17]Stanford, B. K., and Dunning, P. D., "Optimal Topology of Aircraft Rib and Spar Structures," *Journal of Aircraft*, Vol. 52, No. 4, 2015, pp. 1298-1311.

[18]Stanford, B. K., Jutte, C. V., and Wieseman, C. D., "Trim and Structural Optimization of Subsonic Transport Wings using Nonconventional Aeroelastic Tailoring," *AIAA Journal*, Vol. 54, No. 1, 2016, pp. 293-309.

[19]Strauch, G. J., "Integrated Multi-Disciplinary Design of a Sailplane Wing," *MS Thesis*, Virginia Polytechnic Institute and State University, December 1985.

[20]Grossman, B., Gurdal, Z., Strauch, G. J., Eppard, W. M., and Haftka, R. T., "Integrated Aerodynamic/Structural Design of a Sailplane Wing," *Journal of Aircraft*, Vol. 25, No. 9, 1988, pp. 855-860.

[21]Unger, E. R., "Integrated Aerodynamic-Structural Wing Design Optimization," *PhD Dissertation*, Virginia Polytechnic Institute and State University, March 1992.

[22]Gallman, J. W., Smith, S. C., and Kroo, I. M., "Optimization of Joined-Wing Aircraft," *Journal of Aircraft* Vol. 30, No. 6, 1993, pp. 897-905.

[23]Wakayama, S., and Kroo, I. M., "Subsonic Wing Design Using Multidisciplinary Optimization," AIAA 94-4409, 5th AIAA/NASA/USAF/ISSMO Symposium on Multidisciplinary Analysis and Optimization, Panama City Beach, Florida, 7-9 September 1994.

[24]McCullers, L. A., "Aircraft Configuration Optimization Including Optimized Flight Profiles," *Proceedings of the Symposium on Recent Experiences in Multidisciplinary Analysis and Optimization*, NASA CP-2327, 1984, pp. 396-412.

[25]Balabanov, V., Kaufman, M., Giunta, A. A., Haftka, R. T., Grossman, B., Mason, W. H., and Watson, L. T., "Developing Customized Wing Weight Function by Structural Optimization on Parallel Computers," AIAA 96-1336, 37th AIAA/ASME/ASCE/AHS/ASC Structures, Structural Dynamics, and Materials Conference, Salt Lake City, Utah, 15-17 April 1996.

[26]Hutchison, M. G., Unger, E. R., Mason, W. H., Grossman, B., and Haftka, R. T., "Variable-Complexity Aerodynamic Optimization of a High-Speed Civil Transport Wing," *Journal of Aircraft*, Vol. 31, No. 1, 1994, pp. 110-116.

[27]Baker, M., and Giesing, J., "A Practical Approach to MDO and its Application to an HSCT Aircraft," AIAA 95-3885, 1st AIAA Aircraft Engineering, Technology and Operations Congress, Los Angeles, California, 19-21 September 1995.

[28]Huang, X., Dudley, J., Haftka, R. T., Grossman, B., and Mason, W. H., "Structural Weight Estimation for Multidisciplinary Optimization of a High-Speed Civil Transport," *Journal of Aircraft* Vol. 33, No. 3, 1996, pp. 608-616.

[29]Adelman, H. M., and Mantay, W. R., "Integrated Multidisciplinary Design Optimization of Rotorcraft," NASA TM-101642, July 1989.

[30]Friedmann, P. P., "Impact of Structural Optimization with Aeroelastic/Multidisciplinary Constraints on Helicopter Rotor Design," AIAA 92-1001, Aerospace Design Conference, Irvine, California, 3-6 February 1992.

[31]Prandtl, L., "Über Tragflügel kleinsten induzierten Widerstandes," *Zeitschrift für Flugtechnik und Motorluftschiffahrt*, Vol. 11, 1933, pp. 305-306.

[32]Jones, R. T., "The Spanwise Distribution of Lift for Minimum Induced Drag of Wings Having a Given Lift and a Given Bending moment," NACA TR-2249, December 1950.

[33]Gopalarathnam, A., and Norris, R. K., "Ideal Lift Distributions and Flap Angles for Adaptive Wings," *Journal of Aircraft*, Vol. 46, No. 2, 2009, pp. 562-571.

[34]Klein, A., and Viswanathan, S. P., "Minimum Induced Drag of Wings with Given Lift and Root-Bending Moment," *Zeitschrift fur Angewandte Mathematik und Physik*, Vol. 24, 1973, pp. 886-892.

[35]Klein, A., and Viswanathan, S. P., "Approximate Solution for Minimum Induced Drag of Wings with Given Structural Weight," *Journal of Aircraft*, Vol. 12, No. 2, 1975, pp. 124-126.

[36]McGeer, T., "Wing Design for Minimum Drag with Practical Constraints," *Journal of Aircraft*, Vol. 21, No. 11, 1984, pp. 879-886.

[37]Hunsaker, D. F., Phillips, W. F., and Joo, J. J., "Designing Wings with Fixed Twist for Minimum Induced Drag," AIAA 2017-1419, 55th AIAA Aerospace Sciences Meeting, AIAA SciTech Forum, Grapevine, Texas, 9-13 January 2017.

[38]Iglesias, S., and Mason, W. H., "Optimum Spanloads Incorporating Wing Structural Weight," AIAA 2001-5234, 1st AIAA Aircraft, Technology Integration, and Operations Forum, Los Angeles, California, 16-18 October 2001.

[39]Takahashi, T. T., "Optimum Transverse Span Loading for Subsonic Transport Category Aircraft," *Journal of Aircraft* Vol. 49, No. 1, 2012, pp. 262-274.

[40]Pate, D. J., and German, B. J., "Lift Distributions for Minimum Induced Drag with Generalized Bending Moment Constraints," *Journal of Aircraft*, Vol. 50, No. 3, 2013, pp. 936-946.

[41]Prandtl, L., "Tragflügel Theorie," *Nachrichten von der Gesellschaft der Wissescheaften zu Göttingen*, Geschäeftliche Mitteilungen, Klasse, 1918, pp. 451-447

[42]Prandtl, L., "Applications of Modern Hydrodynamics to Aeronautics," NACA 116, June 1921.

[43]Kutta, M. W., "Auftriebskräfte in Strömenden Flüssigkeiten," *Illustrierte Aeronautische Mitteilungen*, Vol. 6, 1902, p. 133.

[44]Joukowski, N. E., "Sur les Tourbillons Adjionts," *Travaux de la Section Physique de la Societe Imperiale des Amis des Sciences Naturales*, Vol. 13, No. 2, 1906.